

NGC 7419 as a template for red supergiant clusters[★]

A. Marco¹ and I. Negueruela¹

Departamento de Física, Ingeniería de Sistemas y Teoría de la Señal. Escuela Politécnica Superior. University of Alicante. Apdo.99
E-03080. Alicante. (Spain)
e-mail: amparo.marco@ua.es

Received; accepted

ABSTRACT

Context. The open cluster NGC 7419 is known to contain five red supergiants and a very high number of Be stars. However, there are conflicting reports about its age and distance that prevent a useful comparison with other clusters.

Aims. We intend to obtain more accurate parameters for NGC 7419, using techniques different from those of previous authors, so that it may be used as a calibrator for more obscured clusters.

Methods. We obtained Strömgren photometry of the open cluster NGC 7419, as well as classification spectroscopy of ~ 20 stars in the area. We then applied standard analysis and classification techniques.

Results. We find a distance of 4 ± 0.4 kpc and an age of 14 ± 2 Myr for NGC 7419. The main-sequence turn-off is found at spectral type B1, in excellent agreement. We identify 179 B-type members, implying that there are more than $1200 M_{\odot}$ in B stars at present. Extrapolating this to lower masses indicates an initial cluster mass of between 7000 and 10000 M_{\odot} , depending on the shape of the Initial Mass Function. We find a very high fraction ($\approx 40\%$) of Be stars around the turn-off, but very few Be stars at lower masses. We also report for the first time a strong variability in the emission characteristics of Be stars. We verified that the parameters of the red supergiant members can be used to obtain accurate cluster parameters.

Conclusions. NGC 7419 is sufficiently massive to serve as a testbed for theoretical predictions and as a template to compare more obscured clusters. The distribution of stars above the main-sequence turn-off is difficult to accommodate with current evolutionary tracks. Though the presence of five red supergiants is marginally consistent with theoretical expectations, the high number of Be stars and very low number of luminous evolved B stars hint at some unknown physical factor that is not considered in current synthesis models.

Key words. open cluster and associations: individual: NGC 7419 - stars: Hertzsprung-Russell (HR) and C-M diagrams, early-type, evolution, emission-line, Be, supergiant - techniques:photometric and spectroscopic

1. Introduction

Open clusters are excellent laboratories for the study of stellar evolution, where we can find rare evolutionary phases in their natural environment. In addition, most massive stars are found in open clusters, because their short lifetimes prevent them from drifting into the field. Unfortunately, the most massive (and interesting) clusters are usually affected by very heavy foreground extinction, makes it difficult and very expensive in telescope time to study them. Very detailed study of accessible open clusters can provide us with valuable information to interpret the much poorer datasets available for very heavily reddened clusters.

NGC 7419 is an open cluster located in Cepheus, near the Galactic plane ($l=109^{\circ}$, $b=1^{\circ}.14$). Its spatial extent is very well defined, with a strong concentration towards the centre and little foreground contamination (Joshi et al. 2008). Beauchamp et al. (1994) estimated its distance, age, and mass function, based on *UBV* CCD photometry and a comparison with the isochrones of Maeder (1990). They obtained a distance of 2.3 kpc, an age of 14 ± 2 Myr, and a mass function that satisfies the Salpeter form. Their photometry was not calibrated with standard stars, but with the photometric sequence of the nearby cluster NGC 7510. Turner et al. (1983) had noted that the same procedure had led to

large systematic differences in $(U - B)$ in the study of the nearby open cluster Mrk 50.

More recently, Subramanian et al. (2006) also presented *UBV* photometry of the cluster, finding an age of 25 ± 5 Myr and a distance of 2.9 kpc. Joshi et al. (2008) estimated, from *UBVRI* photometry, an age of 23 ± 3 Myr and a distance of 3.3 kpc. Unfortunately, there are very large systematic differences between the photometric values reported in these three works. Joshi et al. (2008) and Subramanian et al. (2006) present substantial differences in $(U - B)$ and $(B - V)$ with respect to Beauchamp et al. (1994), which may have some dependence on the observed colours. There are, moreover, important differences between Joshi et al. (2008) and Subramanian et al. (2006), which do not seem to depend on the observed colours, but reach ~ 0.2 mag in $(U - B)$ for many stars. The reasons for these differences are unclear. They may be related to the high reddening towards the cluster, perhaps combined with the choice of calibration. Indeed, of the three works, Joshi et al. (2008) is the only one to calibrate the photometry with Landolt standards.

Based on photometric searching techniques, Pigulski & Kopacki (2000) determined the fraction of Be stars to total number of B-type stars to be $36 \pm 7\%$ among cluster members brighter than $R_C = 16.1$ mag. Such a high fraction of Be stars places NGC 7419 in the small group of clusters very rich in Be stars, such as NGC 663 in the Milky Way, NGC 330 in the Small Magellanic Cloud (SMC), and NGC 1818A in the Large Magellanic Cloud (LMC). This high fraction of Be stars

[★] Partially based on observations collected at the Nordic Optical Telescope and the William Herschel Telescope (La Palma) and at the 1.93-m telescope at Observatoire de Haute Provence (CNRS), France.

has been confirmed by Subramanian et al. (2006) using slitless spectroscopy and by Joshi et al. (2008) using $H\alpha$ photometry. Malchenko & Tarasov (2011) obtained intermediate-resolution spectroscopy around the $H\alpha$ line for most of the candidate Be stars, confirming their nature.

A second peculiarity of NGC 7419 is the presence of five red supergiants (RSGs) as confirmed radial velocity members of the cluster (Beauchamp et al. 1994). Until recently, this was the highest number of RSGs in a Galactic cluster¹. Beauchamp et al. (1994) and Caron et al. (2003) noticed that this high number of RSGs was not accompanied by any blue supergiant. This proportion is at odds with what is generally found in Galactic open clusters, where blue supergiants outnumber RSGs by a factor ~ 3 (Eggenberger et al. 2002).

In recent years, several clusters of RSGs have been discovered towards the Scutum Arm tangent (Figer et al. 2006, Davies 2007, Clark et al. 2009a). These clusters are so heavily obscured that their population of intrinsically blue stars have not been found yet, and only the RSGs have been observed as bright sources in the near-infrared. Population synthesis models indicate that, given the rarity of RSGs, the clusters must contain very large stellar populations. Simulations by Clark et al. (2009b) predict a stellar mass of about 10^4 for each 1–3 RSGs at 10 Myr and 3–5 RSGs at 20 Myr. NGC 7419 offers the opportunity of studying a cluster with a moderately high number of RSGs whose population of B-type stars can be characterised in detail.

In this paper, we determine the fundamental parameters of NGC 7419 using techniques different and more accurate than those of previous authors: Strömgren photometry and intermediate-resolution spectroscopy in the classification region. In view of the very discrepant photometric measurements reported in previous studies, we have decided to try intermediate-band Strömgren photometry which, if correctly calibrated, may allow easy individual dereddening of stellar colours and give accurate photometric spectral types. Intermediate-resolution spectroscopy allows spectral classification that serves to test the accuracy of dereddening procedures and photometric results.

The paper is organised as follows. In Section 2, we describe the photometric and spectroscopic runs in which data were gathered for this work. In Sections 3.1.1 and 3.1.2, we derive spectral types for the brightest blue members of the cluster and the red supergiant members, while in Section 3.1.3 we present evidence for variability in Be stars. In Section 3.2, we use our Strömgren photometry to estimate the cluster parameters, and then calculate the cluster mass in Section 3.3. Finally, in Section 4, we compare our results to those of previous studies and interpret them in view of theoretical expectations and comparison to other clusters, highlighting the role of NGC 7419 as a template for more obscured clusters.

2. Observations and data

In this work, we present Strömgren photometry and multi-epoch spectroscopy of NGC 7419 for the first time. Seven different campaigns of spectroscopic observations have been carried out over the past ten years. We began in 2001 by taking slit spectra of stars catalogued as Be by Pigulski & Kopacki (2000) with the 1.93-m telescope at the Haute Provence Observatory (France) and the Carelec spectrograph. In 2004, we had an observation

run to take photometry and spectroscopy with the 2.6-m Nordic Optical Telescope (NOT, La Palma, Spain). The telescope was equipped with the imager and spectrograph ALFOSC. On this occasion, the weather conditions were not photometric and we could only take slit spectra of the brightest stars and slitless images to detect emission-line stars. In 2005, we had another run at the same telescope. On that occasion, weather conditions were excellent and we could take photometric observations. In addition, we took more slit spectra of bright members. Spectra of the red supergiant members of the cluster were taken in 2007 and 2009 with the William Herschel Telescope and ISIS. In 2008 and 2011, we obtained slitless images again to detect emission-line stars with the NOT, and in 2010 we took a few more slit spectra. With this large collection of data, we are able to confirm the extremely high fraction of Be stars, find evidence of variability in many of them, and determine spectral types for the brightest members.

2.1. Photometry

We obtained Strömgren photometry of the open cluster NGC 7419 using ALFOSC on the Nordic Optical Telescope at the Roque de los Muchachos Observatory (La Palma, Spain) on the night of October 3, 2005. ALFOSC allows observations in different modes. In imaging mode the camera covers a field of $6'5 \times 6'5$ and has a pixel scale of $0'19/\text{pixel}$. For each frame, we obtained two series of different exposure times in each filter to achieve accurate photometry for a broad magnitude range. The central position for the cluster and the exposure times are presented in Table 1.

Standard stars were observed the same night in the clusters NGC 869, NGC 884, NGC 6910, and NGC 1502 using exposure times suitable to obtain good photometric values for all stars selected as standards in these clusters. The central positions for the clusters and the exposure times are presented in Table 1.

The choice of standard stars for the transformation is a critical issue in $uvby$ photometry (Delgado & Alfaro 1989). Transformations made only with unreddened stars introduce large systematic errors when applied to reddened stars, even if the colour range of the standards brackets that of the programme stars (Manfroid & Sterken 1987, Crawford 1994).

We have been carrying out CCD Strömgren photometry of open clusters for years and have always been limited by the scarcity of suitable secondary standard stars. To resolve this problem, we built a list of non-variable and non-peculiar (at least, not reported as such in the literature) candidate stars in different clusters observed with the same Kitt Peak telescopes and instrumentation used to define the $uvby$ (Crawford & Barnes 1970) and $H\beta$ (Crawford & Mander 1966) standard systems, so that there is no doubt that the photometric values are in the standard systems.

A preliminary list of standard stars was presented in Marco & Bernabeu (2001), but dedicated searches for variable stars in the selected open clusters have resulted in the identification of several new variables (Huang & Gies 2006, Saesen et al. 2010a;b). After cleaning the original list, we provide in Table 2 a selection of standards that are almost certainly not variable. The list of adopted standard stars and their photometric data to be used in the transformations of CCD Strömgren photometry of open clusters are given in Table 2. In this run we used only standard stars in NGC 6910, NGC 1502, NGC 884, and NGC 869.

¹ There are five RSGs associated with NGC 884, but four of them are located in the extended halo or association surrounding the cluster (Mermilliod et al. 2008).

Table 1. Log of the photometric observations taken at the NOT in October 2005.

Name	RA(J2000)	Dec(J2000)
NGC 7419	22h 54m 18.7s	+60°48'49"
NGC 6910	20h 23m 10.6s	+40°46'22.4"
NGC 1502	04h 07m 40.4s	+62°20'59.1"
NGC 869	02h 19m 4.4s	+57°08'7.8"
NGC 884	02h 22m 0.6s	+57°08'42.1"

Filter	Exposure times(s)	
	Long times	Short times
NGC 7419		
<i>u</i>	1800	400
<i>v</i>	1000	200
<i>b</i>	600	120
<i>y</i>	120	30
NGC 6910		
<i>u</i>	30	10
<i>v</i>	12	5
<i>b</i>	10	3
<i>y</i>	5	2
NGC 1502		
<i>u</i>	–	10
<i>v</i>	–	5
<i>b</i>	–	3
<i>y</i>	–	2
NGC 869 & NGC 884		
<i>u</i>	–	5
<i>v</i>	–	3
<i>b</i>	–	1
<i>y</i>	–	1

Notes. Cluster coordinates are taken from the WEBDA database (<http://www.univie.ac.at/webda>).

The bias and flat-field corrections of all frames was performed with IRAF² routines. Photometry was obtained by point-spread function (PSF) fitting using the DAOPHOT package (Stetson 1987) provided by IRAF. The apertures used are of the order of the full width at half maximum (FWHM). In this case, we used a value of three pixels for each image in all filters. To construct the PSF empirically, we automatically selected bright stars (typically 25 stars). After this, we reviewed the candidates and discarded those not fulfilling the requirements for a good PSF star. Once we had a list of PSF stars (≈ 20), we determined an initial PSF by fitting the best function of the five options offered by the PSF routine inside DAOPHOT. We allowed the PSF to be variable (in order 2) across the frame to take into account the systematic pattern of PSF variability with the position on the chip. We needed to perform an aperture correction of 15 pixels for each frame in all filters.

The atmospheric extinction corrections were performed using the RANBO2 program, which implements the method described by Manfroid (1993). Finally, we obtained the instrumental magnitudes for all stars.

Using the standard stars, we transformed the instrumental magnitudes to the standard system using the PHOTCAL pack-

² IRAF is distributed by the National Optical Astronomy Observatories, which are operated by the Association of Universities for Research in Astronomy, Inc., under cooperative agreement with the National Science Foundation

age inside IRAF. We implemented the following transformation equations, after Crawford & Barnes (1970a):

$$V = 15.565 - 0.021(b - y) + y_i \quad (1)$$

$$\pm 0.011 \pm 0.020$$

$$(b - y) = 1.022 + 0.870(b - y)_i \quad (2)$$

$$\pm 0.014 \pm 0.024$$

$$c_1 = 0.362 + 0.933c_{1i} - 0.040(b - y) \quad (3)$$

$$\pm 0.025 \pm 0.029 \pm 0.043,$$

where each coefficient is given with the error resulting from the transformation.

The number of stars that we could detect in all filters is limited by the long exposure in the *u* filter. We identify all stars with good photometry photometric errors ≤ 0.04 in all four filters on the image in Figures 1 and 2. In Table 3, we list their coordinates in J2000 (from Joshi et al. 2008) and their identification with objects in the WEBDA database. The designation of each star is given by the number indicated on the images (Fig. 1 and Fig. 2). We have photometry for 202 stars in the field. In Table 3, we list the values of V , $(b - y)$ and c_1 with the assigned photometric errors and the number of measurements for each magnitude, colour, or index. The error assigned is the standard deviation for star with three or four measurements and the photometric errors from DAOPHOT for stars with only one measurement, with the errors in the colour indices calculated through error propagation.

We completed our dataset with JHK_s photometry from the 2MASS catalogue (Skrutskie et al. 2006). In Table 4 we show the 2MASS photometric values for the stars confirmed as cluster members in Section 3.2 that have good-quality photometric flags and photometric errors below 0.05 mag in all 2MASS filters.

2.2. Spectroscopy

Most of the spectroscopic observations were obtained with ALFOSC in spectroscopic mode during the 2004 and 2005 NOT runs. A few spectra of selected stars were taken in service mode in November 2010 (on the nights of November 10 and November 23). During the 2004 run, the seeing was quite poor, except on the night of November 3. We resorted to using a 1''.8 slit on both November 2 and 4. For all other ALFOSC observations, we used 1''.0 slits.

Our primary setup was grism #16 for classification spectroscopy. This grism covers the 3500–5060 Å range with a nominal dispersion of 0.8 Å/pixel. The resolving power, measured on arc lines, is ~ 1500 with the 1''.0 slit. With the 1''.8 slit, it even reaches $R \sim 1000$.

In the 2004 run, a few objects were observed with grism #7, which covers the 3850–6850 Å with a nominal dispersion of 1.5 Å/pixel. The resolving power is ~ 550 with the 1''.8 slit and ~ 700 with the 1''.0 slit. In the 2005 run, we observed a few fainter stars with grism #14. This grism covers the 3275–6125 Å range with a nominal dispersion of 1.4 Å/pixel. The resolving power with the 1''.0 slit is $R \sim 800$. Even though this grism does not include the region of H α , it has a much higher throughput in the blue than grism #7, and it was thus preferred to obtain classification spectra for faint stars. Finally, in the 2010 service observations, two objects were observed with grism #8. This grism covers the 5825–8350 Å range with a nominal dispersion of 1.3 Å/pixel, giving a resolving power of $R \approx 1300$. Wavelength calibration was achieved by using ThAr arc lamp

Table 2. Standard stars with their catalogued values and spectral types taken from the literature.

Star	V	$b - y$	m_1	c_1	$H\beta$	spectral type
NGC 869						
782	9.450	0.268	-0.053	0.150	2.618	-
800	12.250	0.316	-0.031	0.404	2.701	-
837	14.080	0.393	0.000	0.918	2.801	-
867	10.510	0.393	0.161	0.375	2.613	-
935	14.020	0.362	-0.004	0.854	2.802	-
950	11.290	0.318	-0.048	0.214	2.642	B2V
978	10.590	0.305	-0.039	0.177	2.643	B2V-B1.5V
980	9.650	0.290	-0.054	0.167	-	B1.5V
991	11.320	0.329	-0.062	0.275	-	B2V
1015	10.570	0.225	0.033	0.741	2.772	B8V
1078	9.750	0.316	-0.065	0.167	2.610	B1V
1181	12.650	0.372	-0.034	0.379	2.718	-
1187	10.820	0.348	-0.063	0.212	2.648	B2IV
NGC 884						
2005	13.560	0.35	-0.013	0.713	2.750	-
2139	11.380	0.255	-0.033	0.196	2.649	B2V
2147	14.340	0.406	-0.050	1.002	2.863	-
2167	13.360	0.352	-0.056	0.627	2.752	-
2196	11.570	0.250	-0.006	0.210	2.670	B1.5V
2235	9.360	0.316	-0.088	0.150	2.611	-
2330	11.420	0.267	-0.050	0.277	2.640	-
2572	10.020	0.311	-0.091	0.197	2.620	-
NGC 6910						
10	10.750	0.100	0.150	1.040	2.909	-
20	10.900	0.770	0.420	0.430	2.555	-
24	11.720	0.660	-0.140	0.220	2.647	B1V
21	11.730	0.590	-0.100	0.220	2.652	B1V
28	12.220	0.590	-0.110	0.330	2.679	-
172?	13.900	0.710	-0.080	0.590		
NGC 1502						
30	9.650	0.475	-0.096	0.157	2.628	B1 V
35	10.460	0.422	-0.052	0.265	2.661	B3 V
41	13.030	0.552	0.003	1.232	2.874	
42	12.590	0.510	-0.078	0.960	2.770	
45	11.460	0.475	-0.065	0.526	2.723	
49	10.710	0.436	-0.058	0.316	2.656	B3 V
NGC 1039						
267	11.960	0.303	0.138	0.481	2.678	
274	9.740	0.086	0.176	0.973	2.890	A2.5V
278	11.820	0.144	0.198	0.900	2.855	
284	10.760	0.151	0.194	0.894	2.848	
294	11.220	0.176	0.204	0.796	2.817	
301	10.030	0.066	0.152	1.013	2.916	
303	9.950	0.055	0.163	1.021	2.908	

Notes. Photometric data are taken from Crawford et al. (1970) and Johnson & Morgan (1955) for NGC 869 and NGC 884; Perry et al. (1978) for NGC 2169; Crawford et al. (1977) for NGC 6910; Canterna et al. (1979) for NGC 1039, and Crawford (1994) for NGC 1502. Spectral types, when available, are taken from Schild (1965), Slettebak (1968) and Johnson & Morgan (1955) for NGC 869 and NGC 884; Perry et al. (1978) for NGC 2169; Morgan & Harris (1956) and Hoag & Applequist (1965) for NGC 6910; Abt & Levato (1977) for NGC 1039, and Hoag & Applequist (1965) for NGC 1502.

spectra, taken between the exposures. The rms for the wavelength solution is ≈ 0.2 pixels for all grisms.

During the 2004 run, we also obtained slitless spectroscopy of the field by combining the low-resolution grism #4 with the Bessel R -band filter. Slitless fields were taken at three different orientations to minimise source overlapping. More slitless observations were taken during other runs in August 2008 and September 2011.

Low-resolution spectra of some of the brightest Be candidates were taken on 2001 July 1 with the 1.93-m telescope at

Haute Provence Observatory (France) and the Carelec spectrograph, equipped with an EEV42 CCD. A $1'8$ slit was used, giving a resolving power $R \approx 1000$ over the 3800–6800 range, though the signal-to-noise ratio (S/N) is very low in the blue.

Spectra of the red supergiants in the far-red were taken on 2007 August 21 using the red arm of the ISIS double-beam spectrograph, mounted on the 4.2 m William Herschel Telescope (WHT) in La Palma (Spain). The instrument was fitted with the R600R grating and the Red+ CCD. This configuration covers the 7600-9000Å range in the unvignetted section of the CCD with

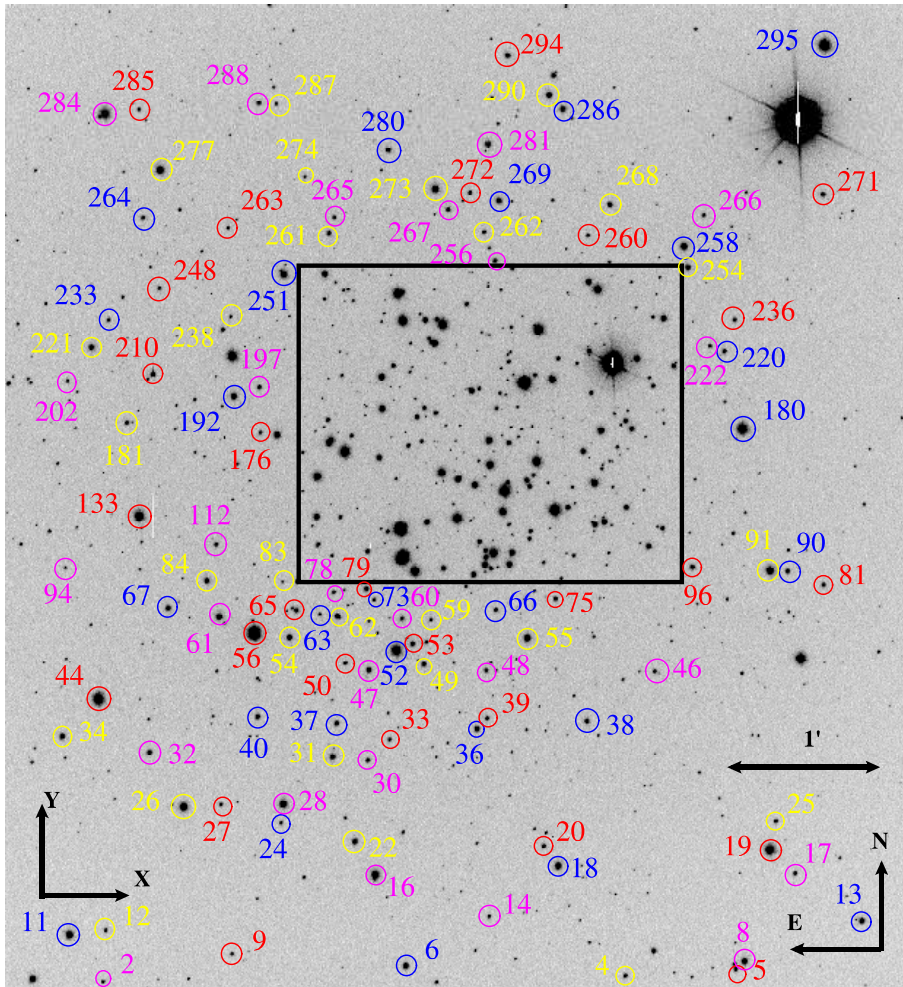


Fig. 1. Finding chart for stars with photometry in the field of NGC 7419. The image is one of our V-band frames. Stars inside the rectangle (which approximately defines the cluster core) are marked in Fig. 2. Each star is identified by the nearest marker in the same colour as the circle around it. The origin of the coordinates is located at the bottom-left corner of each frame.

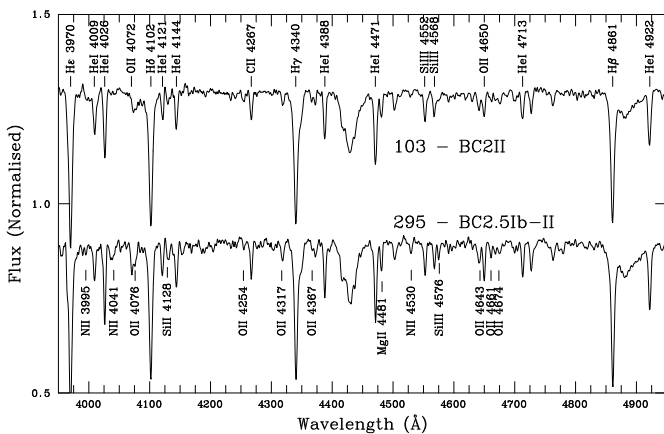


Fig. 3. Classification spectra of the two brightest blue cluster members obtained with the NOT. Note the lower resolution of the top spectrum, observed with a $1''.8$ slit. The most prominent stellar features are marked. The strong diffuse interstellar bands at 4428, 4502, 4726, 4760, and 4882Å are not marked.

a nominal dispersion of $0.5\text{\AA}/\text{pixel}$. The CCD was binned by a factor of two in the spectral direction and a $1''.2$ slit was used. The resolution element is expected to be about four unbinned

pixels. This was checked by measuring the width of arc lines, which is on average $\approx 2.1\text{\AA}$. The resolving power of our spectra is $R \approx 4000$. The observation of the star B139 was taken on 2009 September 13 with the same configuration and a $1''.5$ slit.

All spectroscopic data were reduced using the Starlink software packages CCDPACK (Draper et al. 2000) and FIGARO (Shorridge et al. 1997). We used standard procedures for bias subtraction and flat-fielding (using internal halogen lamps). The spectra were normalised to the continuum using DIPSO (Howarth et al. 1998).

3. Results

3.1. Spectroscopy

In total, we obtained blue spectra for ~ 40 stars, but not all of them are useful for spectral classification. For the objects with spectra of sufficient quality for an accurate spectral classification, spectral types are given in Table 5.

3.1.1. Spectral classification

The brightest blue stars in the cluster are star 103, in the core region, and star 295, an outlier to the northwest. Their spectra, displayed in Fig. 3, are very similar. They are rather luminous stars.

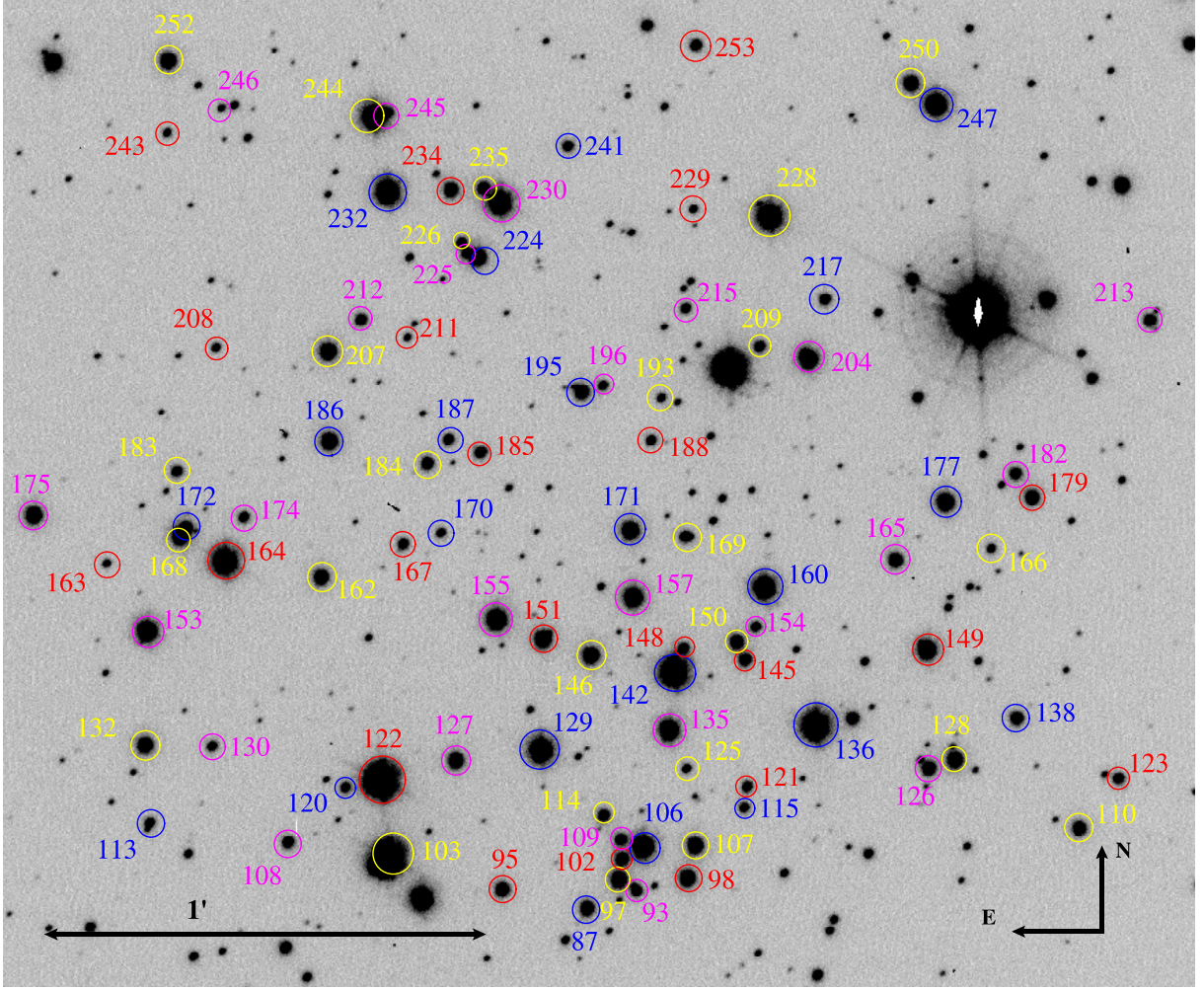


Fig. 2. Finding chart for stars with photometry in the central part of NGC 7419. The image is one of our V-band frames. Each star is identified by the nearest marker in the same colour as the circle around it. The origin of the coordinates is located at the bottom-left corner of the frame.

The spectral types of early-B stars are commonly determined by comparing ratios of different Si ions. In these two stars, Si IV is undetectable, while Si III lines are strong and Si II lines are moderately strong. This places our objects close to the B2 spectral type (Walborn & Fitzpatrick 1990). The Si II 4128–30 Å doublet is too weak compared to the neighbouring He I lines for a B3 spectral type, while the O II spectrum is too weak for B1. The main luminosity criterion around B2 is the ratio of Si III 4552 Å to H I 4387 Å (Walborn & Fitzpatrick 1990). In our objects, it indicates a luminosity class of II or Ib. The very strong C II 4267 Å line could suggest that the spectral type is B2.5, also supported by the relatively high ratio of Mg II 4481 Å to the Si III lines (Walborn & Fitzpatrick 1990). However, at this spectral type the N II spectrum should be close to its maximum, but N lines are very weak or absent in our targets. N II 3995 Å is very weak compared to He I 4009 Å, while N II 4631 Å is absent, when it should be stronger than O II 4650 Å. This strongly indicates that both stars are nitrogen-deficient. If this is the case, they are likely to be carbon-enhanced as well. We assign nominal spectral types BC2 II for star 103 and BC2.5 Ib-II for star 295, but note that with the uncertainties discussed, both stars could be given identical classifications, within the B2–B2.5 range and a luminosity class very slightly lower than necessary to be a supergiant.

The spectra of several other bright cluster members are shown in Fig. 4. The next-brightest blue star is star 180. This object is clearly earlier than any other member, as shown by the presence of Si IV 4089 Å, or the prominent C III+O II 4650 Å, which is as strong as H I 4387 Å. Its position in the photometric colour-magnitude diagram (CMD) (see Fig. 8) confirms that this object is a blue straggler. The prominent C III+O II 4070 Å, as deep as He I 4144 Å, points to a spectral type as early as B0.5 III, in good agreement with the c_0 value, even if He II 4686 Å is not seen at this resolution. However, again, there is evidence for some anomaly, as nitrogen lines should not be seen at this spectral type. N II 3995, 4041, 4530, and 4631 Å are present, though, as well as several weak lines between 4601–4621 Å. Therefore the star is likely to be slightly nitrogen-enhanced. Nitrogen enhancement is usually accompanied by carbon deficiency, which does not seem to be present. In view of this, we classify the star as B0.5N III, though we cannot rule out the possibility that it is slightly later and more luminous, around B1 II.

The brightest Be star is star 136, which presents heavy veiling by emission lines. Its spectral type is close to B1 III. It seems to be slightly less luminous, but this may be due to the broad shallow lines typical of Be stars. Star 52 has a similar spectral type, but does not present emission lines. Star 142 is slightly

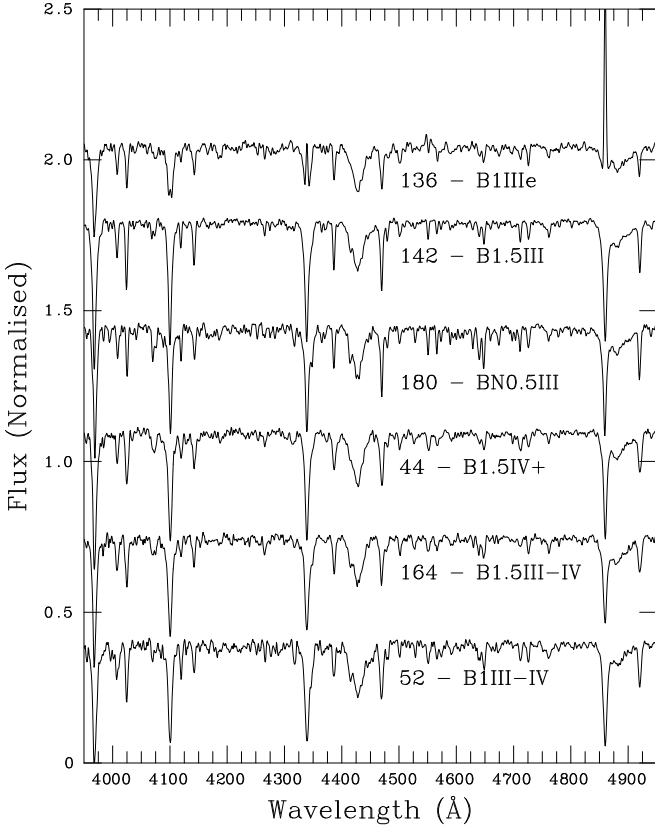


Fig. 4. Classification spectra of several bright blue cluster members.

later, as shown by the stronger C Π 4267Å line and the presence of some weak N Π lines. We assign a spectral type B1.5 III. The Be star 164 has a similar spectral type. This later star showed emission lines until 2005, but presents a completely normal spectrum in 2010 (displayed).

Star 44 is an interesting case. We have three spectra of this object (2004, 2005, and 2010), all looking different. The best one, from 2010 (displayed), shows a normal B1.5 IV star. This spectral type does not seem to agree with its brightness. Moreover, the 2004 spectrum, though rather noisier, showed evidence for a later spectrum, with strong Si Π 4128–30Å and C Π 4267Å and weak Si III. We speculate that the star is perhaps a binary system, containing a B1.5 IV and a \sim B3 III star, though more observations are needed to confirm this. The star displayed some emission infilling in H α in the 2001 spectrum, but no evidence for Be characteristics in any of the blue spectra. Caron et al. (2003) classified this star as B4 III based on its far-red spectrum, corroborating the presence of a late-type companion. They remarked that the Paschen lines were flat-bottomed, an effect that they attributed to weak Be characteristics, but that could also be due to the presence of two stellar spectra. Malchenko & Tarasov (2011) observed weak double-peaked H α in this object in June 2006.

The spectra of fainter stars have a lower resolution or a lower S/N (or both), but their features are still good enough for rough classifications, accurate to ± 1 spectral type. There is a number of relatively bright Be stars (129, 133, 228, 230, 232, and 244) that we classify as B1–1.5 IV. These objects represent the top of the main sequence, and the concentration of Be stars seems to be very high in this magnitude range. Around $V = 15$, we

Table 5. Spectral types for stars in NGC 7419 with classification spectra.

Star	Spectral type
Red supergiants	
B139	M1 Iab
B435	M1.5 Iab
B696=122	M1.5 Iab
B921=56	M0 Iab
B950	M7.5 I
Be stars	
129	B1.5 IVe
133	B1.5 IVe
136	B1 IIIe
155	B1 Ve
164	B1.5 III-IVe
207	B2 Ve
228	B1 IVe
230	B1.5 IVe
232	B1 IVe
244	B1 IVe
Other bright blue stars	
44	B1.5 IV+?(e)
52	B1 III-IV
91	B1 V
103	BC2 II
106	B1 IV
142	B1.5 III
160	B1.5 IV
180	BN0.5 III
247	B2 III-IV
295	BC2.5 Ib-II

find a number of stars without emission lines (e.g., 106, 160) that are definitely not giants. These objects with spectral type \approx B1 IV indicate the turn-off age of the cluster. Unfortunately, the quality of the spectra does not allow us to give high weight to the luminosity-class determination. Star 247, on the other hand, shows a very weak O Π spectrum, and it may be a more evolved star, B2 III-IV, its faintness explained by higher-than-average reddening. Unfortunately, its spectrum has a very low S/N.

A peculiar case is star 91. This is the most reddened B-type star in the cluster. Even though it is quite faint in the B band, its dereddened magnitudes indicate $M_V = -4.9$, far too bright for a main-sequence star. We only have a low-resolution spectrum of this object, which suggests a spectral type B1 V. Despite the low resolution, we should expect to see some metallic lines in the spectrum if the object were a B1 III star, as suggested by its absolute magnitude, since the S/N is good (60–80 in the classification region). Perhaps the star is a background object in the Outer or Cygnus arm, but a better spectrum is needed to ascertain this possibility.

3.1.2. Red supergiants

The presence of five red supergiants in NGC 7419 was first noted by Blanco et al. (1955). Using objective-prism infrared spectra, they derived spectral types between M2 and M3.5 for four of them, and M7 for the last one. This later-type star was observed to be photometrically variable. Fawley & Cohen (1974) took near-infrared photographic spectra of four of the red supergiants, confirming that they all had the same radial velocity. They

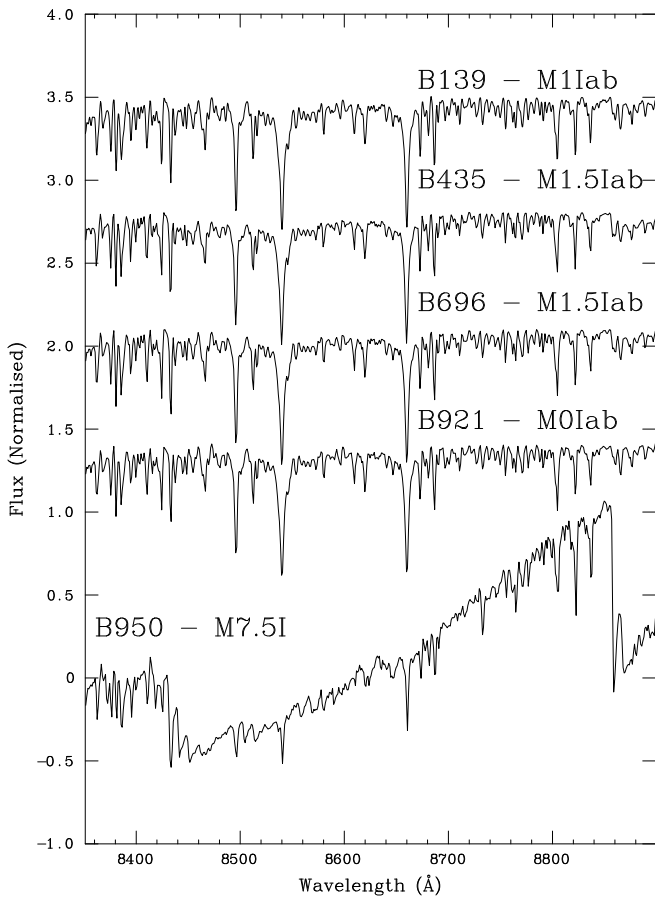


Fig. 5. Spectra of the five red supergiants in NGC 7419, in the region around the Ca II triplet.

classified three of them as M2 Iab (B921, B696, and B435)³, and confirmed the late spectral type of B950, which they refined to M7.5 I. Finally, Beauchamp et al. (1994) obtained CCD spectra of all five RSGs in the region of the Ca II triplet, confirming that they have radial velocities very similar to blue cluster members. They also confirmed their RSG character by measuring the strength of the Ca II triplet lines.

Figure 5 displays the spectra of the five RSGs around the Ca II triplet. The criteria for spectral classification of RSGs in this region have been summarised by Negueruela et al. (2011). In this range, the spectral type can be determined from the depth of the TiO $\delta(0,0)$ *R*-branch bandhead at 8860Å, which correlates strongly with effective temperature (T_{eff}). B921 has no sign of this bandhead and therefore is around M0. B139, B435, and B696 have weak bandheads that make them earlier than M2. The luminosity class can be estimated from the Ti I/Fe I 8468Å blend and the equivalent width of the Ca II lines, which suggest class Iab for all of them. The high luminosity is also supported by the very high ratios of the 8514Å blend to the Ti I 8518Å line (Keenan & Hynes 1945). However, the blend is still rather weaker than Ti I 8435Å, showing that the luminosity class is not Ia.

B950 is much later, with very strong TiO systems. Classification criteria for RSGs later than M5 have not been de-

³ For the red supergiants, we use the notation of Beauchamp et al. (1994), because only two of them were detected in all filters by our photometry, B696=122 and B921=56.

scribed. Standard stars have not been defined, because late-M supergiants generally show spectral-type variability (Abt 1963). Solf (1978) extended classification criteria to late-M giants in the red region. According to these, at M7, the VO bandhead at 7982Å is of similar strength to the TiO 7820, 7828Å bandheads, while the VO feature at 7961Å is just visible. The VO bandheads at 8538 and 8624Å become first visible at M8 on photographic spectra, with the former being comparable in strength to Ca II 8542Å. Our spectrum of B950 shows much stronger Ca II, a fact attributable to the dependence on luminosity of the Ca II triplet. The 8624Å bandhead is clearly seen, though blended with the 8621Å interstellar band. The 7961Å VO bandhead is also quite strong. In view of this, and allowing for the differences between giants and supergiants, we find the M7.5 I classification fully justified. The resulting classifications are summarised in Table 5.

The classifications for B435, B696, and B950 are fully compatible with previous work. However, B139 and B921 are earlier here. B921 is clearly earlier than any other RSG in the cluster, and given as M0 Iab, against M2.5 I in Blanco et al. (1955) and M2 Iab in Fawley & Cohen (1974). B139 is M1 Iab, against M3.5 I in Blanco et al. (1955). Even though the differences of two spectral subtypes seem large, classification criteria are subtle and the weight of prism spectral types is low. Since most early-M supergiants show stable spectral types, additional observations are needed before spectral variability can be claimed.

3.1.3. Be stars

Previous authors have reported a high percentage of Be stars in NGC 7419 (Pigulski & Kopacki 2000, Subramanian et al. 2006, Joshi et al. 2008). All these references reported single-epoch observations. Be characteristics, on the other hand, are known to be variable on time scales ranging from months to many years (Porter & Rivinius 2003). For the first time, we present multi-epoch spectroscopy of Be stars in NGC 7419, which we complement with all the data available in the literature. Table 6 lists all members of NGC 7419 that have ever been reported to show emission in H α , together with all detections of emission for every star. For each observation or each reference in the literature, we indicate detections, reported non-detections, or lack of definite evidence (which may have many different causes, such as crowding in slitless fields, location outside the field of view of the observations, or lack of the information in the corresponding references). In November 2010, four stars listed in Table 6 were observed in service mode. Classification spectra were obtained for 44 and 164, and showed no sign of emission (shown in Fig. 4). Spectra around H α were taken for 151 and 155 (shown in Fig. 7). Since only four stars were observed, this run is not reported in Table 6.

Using the standard definition of a Be star as a star that has or has had Balmer lines in emission at one time (Porter & Rivinius 2003), we consider any star ever reported as showing emission as a Be star. As can be seen in Figures 8, 9, and 10, Be stars concentrate above and around the main-sequence turn-off, a behaviour observed in many other clusters (McSwain & Gies 2005). The fraction of Be stars to total number (B+Be) is 58% for stars brighter than $V = 15$ (essentially, above the turn-off) and 40% for stars brighter than $V = 17$ (corresponding to spectral type B2 V). Below this limit the number of Be stars is small. Though selection effects might play a role in this low fraction of Be stars at faint magnitudes, we consider this unlikely, because different authors have used H α photometry, which is sensitive at faint

Table 6. Spectroscopic monitoring of Be stars for ten years. The "X" symbol means that we cannot know if the source was displaying emission line because it was outside the field, heavily blended, too faint for detection, or some other reason. "-" means that the star did not show emission in H α . "+" means that the star displayed the H α line in emission.

Name	A ¹	B ²	C ³	D ⁴	E ⁵	F ⁶	G ⁷	H ⁸	I ⁹	K ¹⁰
18	X	X	X	+	X	-	X	+	+	+
30	+	X	X	X	X	+	X	+	+	+
34	-	X	X	X	X	-	X	-	-	+
44	+	+	X	X	-	-	+	+	-	-
47	+	X	X	+	+	+	+	+	+	+
55	+	X	X	+	X	+	+	+	+	+
61	+	X	X	X	X	-	-	+	-	-
62	+	X	X	+	X	+	+	+	+	+
87	+	X	X	X	X	-	X	+	+	-
96	+	X	+	+	X	+	+	+	+	+
98	+	X	X	X	X	-	-	+	+	-
100	+	X	+	X	X	X	X	X	+	+
107	+	X	X	X	X	-	+	+	-	-
126	+	+	+	X	X	-	X	+	+	-
129	+	X	+	+	+	+	+	+	+	+
133	+	+	X	+	+	+	+	+	+	+
136	+	+	+	+	+	+	X	+	+	+
151	+	+	+	X	X	+	X	+	-	-
153	+	X	X	+	+	+	+	+	+	+
155	+	+	-	-	-	+	+	+	-	+
157	+	X	X	+	X	+	+	+	-	+
164	+	+	+	+	+	+	+	+	-	-
168	+	+	X	+	X	+	X	+	+	+
171	-	X	X	X	X	-	X	-	+	-
175	+	+	X	+	X	+	+	+	+	+
207	+	X	X	+	+	+	+	+	+	+
228	+	+	+	+	+	+	+	+	+	+
230	+	+	+	+	+	+	+	+	+	+
232	+	+	+	+	+	+	+	+	+	+
235	+	X	X	-	X	X	X	X	+	+
244	+	+	+	+	X	+	+	+	+	+
250	+	X	X	X	X	X	+	+	+	+
258	+	X	X	+	X	+	+	+	+	+
260	-	X	X	X	X	-	X	+	+	-
273	X	X	X	X	X	-	X	-	+	-
281	X	X	X	X	X	-	X	-	X	+
290	X	X	X	X	X	-	X	+	+	+
294	X	X	X	X	X	-	X	+	X	+

⁽¹⁾ (Pigulski & Kopacki 2000), ⁽²⁾ 2001(spectra), ⁽³⁾ 2004(spectra),
⁽⁴⁾ 2004(slittless), ⁽⁵⁾ 2005(spectra), ⁽⁶⁾ (Subramanian et al. 2006),
⁽⁷⁾ (Malchenko & Tarasov 2011), ⁽⁹⁾ (Joshi et al. 2008),
⁽⁸⁾ 2008(slittless), ⁽¹⁰⁾ 2011(slittless)

magnitudes. For example, Joshi et al. (2008) claimed to be essentially complete down to $V = 18$ and have a completeness factor of 90% in the cluster halo down to $V = 20$. We must thus conclude that the fraction of Be stars decreases as we move down the main sequence towards late-B types, as found in most clusters containing classical Be stars (McSwain & Gies 2005).

The information displayed in Table 6 fully confirms the variable nature of Be characteristics in many of the stars observed. For example, in 2001, star 164 had H α strongly in emission ($EW = -28\text{\AA}$), while H β was in emission well above the continuum. Its subsequent evolution can be seen in Fig. 6. The emission line gradually disappeared between 2001 and 2005, until the spectrum taken in 2010 (displayed in Fig. 4) shows no

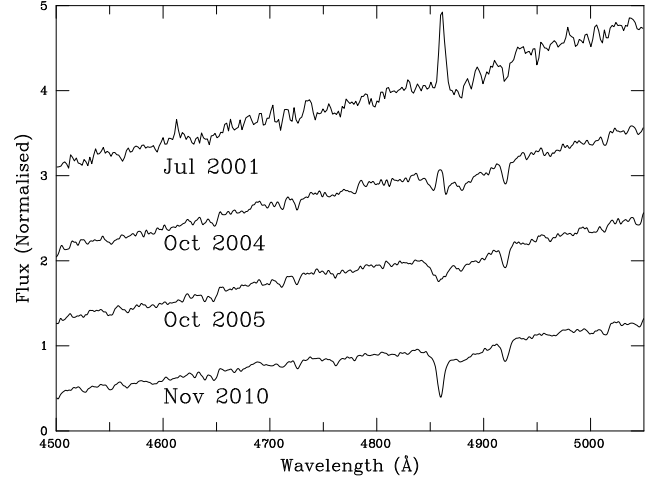


Fig. 6. Spectra of the Be star 164 taken at different epochs and showing the progressive disappearance of emission characteristics.

characteristics that allow its classification as a Be star. H α was still weakly in emission in 2006 (Malchenko & Tarasov 2011). A similar evolution was followed by Star 151. This object displayed strong H α emission ($EW = -25\text{\AA}$) in 2001, but this had decreased strongly by 2004 ($EW = -13\text{\AA}$). Emission from this star was not detected in the slitless spectroscopy either in 2008 and 2011, while the spectrum taken in 2010 (Fig. 7) shows the H α line fully in absorption and lacking any emission component.

More complex evolution has been shown by star 155. Detected as a Be star by Pigulski & Kopacki (2000), it displayed a neutralised H α line (the emission component is strong enough just to mask the photospheric absorption) in its 2001 spectrum. After this, it was not detected in emission in 2004 or 2005, but reappeared as an emission-line star in the 2008 slitless spectrum. Malchenko & Tarasov (2011) had already detected a very weak double-peaked emission in 2006. In November 2010, it displayed a moderately strong double-peaked emission line (Fig. 7), indicative of a circumstellar disk well in the process of reformation.

This sort of variability is typical of classical Be stars, but is not observed in Herbig Be stars. Table 6 shows many other examples of stars that appear to have passed through diskless phases, though they are not as well documented as the examples above. The time-scales implied are typical of classical Be stars with disk disappearance and reformation happening over a few years.

3.2. Observational HR diagram

We started the photometric analysis by plotting the $V/(b - y)$ and V/c_1 diagrams for all stars in our field. To assess the membership of a star, we look at its position in the $V/(b - y)$ and V/c_1 diagrams. We found that in both diagrams, the vast majority of the stars fall along a very well defined main sequence. We considered as non-members the objects that do not fit the main-sequence loci in either of the diagrams, unless they are catalogued as Be stars. Indeed, Be stars have colours different from those of non-emission B stars because of the additional reddening that is caused by the circumstellar envelope, and they tend to have redder ($b - y$) and lower c_1 values than normal B stars (see Figures 8 and 9).

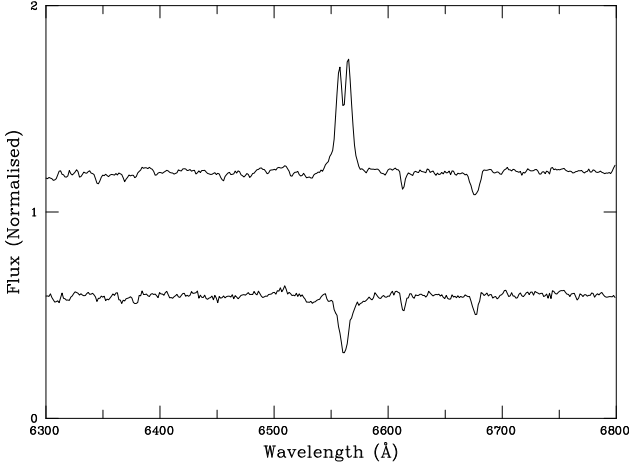


Fig. 7. Intermediate-resolution spectra around $H\alpha$ for 155 (top) and 151 (bottom) in November 2010. These two Be stars have undergone substantial variability during the past ten years, including the complete loss of the envelope. At the time when the spectrum was taken, 155 was reforming its disk.

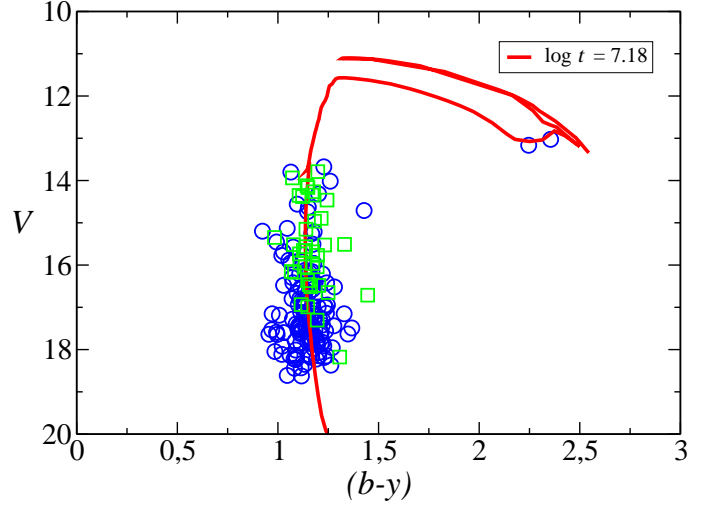


Fig. 9. $V/(b-y)$ diagram for all members in the cluster. Open squares represent the members catalogued as Be stars. The solid line is the isochrone of Marigo et al. (2008) corresponding to $\log t = 7.18$, reddened by $A_V = 5.2$ and displaced to $DM = 13.0$. The isochrone has been reddened taking into account colour effects, following the procedure described in Girardi et al. (2008).

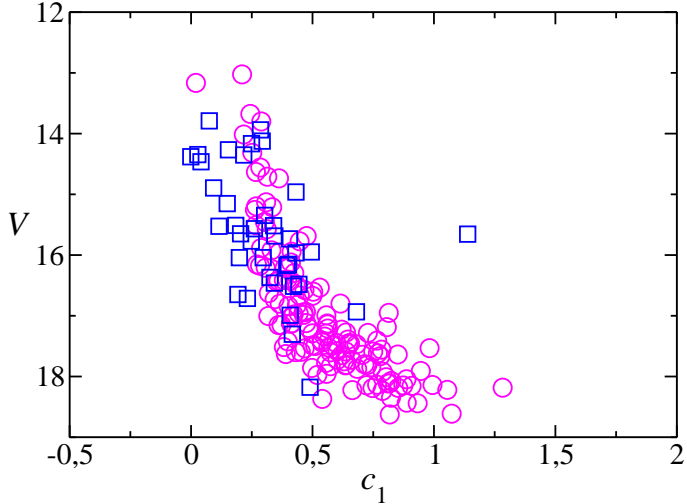


Fig. 8. V/c_1 diagram for all members in the cluster. Open squares represent the members catalogued as Be stars.

We calculated individual reddenings for all cluster members. We followed the procedure described by Crawford et al. (1970), and we used the observed c_1 to predict the first approximation to $(b-y)_0$ with the expression $(b-y)_0 = -0.116 + 0.097c_1$. Then we calculated $E(b-y) = (b-y) - (b-y)_0$ and used $E(c_1) = 0.2E(b-y)$ to correct c_1 for reddening $c_0 = c_1 - E(c_1)$. The intrinsic colour $(b-y)_0$ was then calculated by replacing c_1 with c_0 in the above equation for $(b-y)_0$. Three iterations are enough to reach convergence in the process. Naturally, this procedure only results in physically meaningful values for stars without circumstellar excesses (i.e., not for Be stars). Restricting the analysis to stars that have never been classified as Be stars, we found a moderate degree of differential reddening amongst members. The average value of the colour excess is $E(b-y) = 1.23 \pm 0.12$, where the er-

ror bars are given by the standard deviations of all values⁴. The median value is $E(b-y) = 1.24$.

Using the standard relation $E(b-y) = 0.74E(B-V)$ and taking into account the presence of differential reddening, this average value agrees very well with the $E(B-V) \approx 1.7$ determined by Joshi et al. (2008) and Subramanian et al. (2006)⁵. Our value disagrees from that found by Beauchamp et al. (1994), $E(B-V) \approx 2.0$ even though we found the same age for the cluster (see Section 3.2.2). This confirms the suspicion by Beauchamp et al. (1994) that their $(U-B)$ colours, calibrated against stars in NGC 7510, might suffer from a systematic error.

With the aid of these individual values we calculated the intrinsic colours c_0 and magnitudes V_0 of the normal B-type members. From c_0 and V_0 , we estimated photometric spectral types using the calibration for c_0 from Crawford (1978). The photometric types are displayed in Table 7. For those stars with spectroscopic spectral types (see Table 5), the agreement between photometric and spectroscopic types is excellent, certifying the correctness of the dereddening procedure.

3.2.1. Distance determination

We estimated the distance modulus (DM) to NGC 7419 by fitting the observed V_0 vs. c_0 zero age main-sequence (ZAMS) to the mean calibrations of Perry et al. (1987). We fitted the ZAMS as a lower envelope for most of the members, deriving a best-fit distance modulus of $V_0 - M_V = 13.0 \pm 0.2$ (the error indicates the uncertainty in positioning the theoretical ZAMS and its identification as a lower envelope; see Fig 10). This DM corresponds to a distance of $4.0^{+0.4}_{-0.4}$ kpc. Both Joshi et al. (2008) and Subramanian et al. (2006) found distances around ≈ 3 kpc, but their error bars place our value within 2σ of our determi-

⁴ All colour excesses are within two standard deviations of the average, with the single exception of star 91, showing that the spread in reddening is moderate (see Fig. 11).

⁵ The agreement in the $E(B-V)$ determination between these two references is surprising, since large systematic differences exist between their $(U-B)$ values.

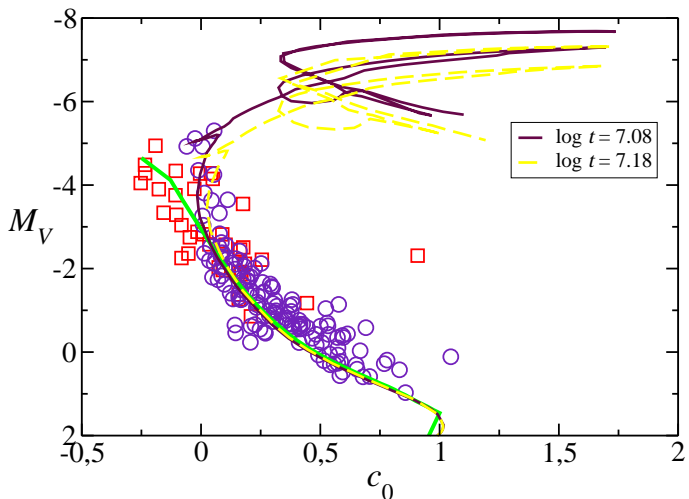


Fig. 10. Absolute magnitude M_V against intrinsic colour c_0 for B-type stars in NGC 7419. Open squares are stars catalogued as Be stars. The thick line represents the ZAMS from Perry et al. (1987). Two isochrones of Marigo et al. (2008), corresponding to $\log t = 7.08$ and $\log t = 7.18$, are labelled with their respective $\log t$.

nation. Our data were individually dereddened while theirs are based on average reddening, but the difference in DM results almost exclusively from the different ages found (see next subsection). Subramanian et al. (2006) and Joshi et al. (2008) used a fit to theoretical isochrones to simultaneously determine the age and distance to the cluster, while we fitted the distance to the observational ZAMS. The difference with respect to the value of Beauchamp et al. (1994) is due to the adoption of a different reddening law.

3.2.2. Age determination

To determine the cluster age, we fitted by eye isochrones in the $V/(b-y)$ (Figure 9) and M_V/c_0 (Figure 10) observational diagrams to the position of the red stars and the turn-off. We used isochrones from Marigo et al. (2008), computed using a Kroupa (1998) initial mass function (IMF) corrected for binaries. The isochrone shown in Fig. 9 was reddened following the procedure described in Girardi et al. (2008), which takes into account colour effects for late-type stars. The reddening procedure uses the extinction law from Cardelli et al. (1989) and O’Donnell (1994) with $R_V = 3.1$.

The M_V/c_0 diagram provides a good fit of the turn-off for the 12 Myr isochrone, once the Be stars are removed. The brightest B stars are close to the end of H-core burning, which agrees very well with their observed spectral types. The turn-off can also be fitted with a slightly older isochrone (15 Myr). The brightest blue stars then appear as blue stragglers, but the fit to the turn-off improves slightly. Spectroscopically, only star 180 (BN0.5 III) is decidedly a blue straggler. Since the dereddening method used to derive c_0 is only valid for early-type stars, the red supergiants 56 and 122 do not appear in this diagram.

The two red supergiants appear in the $V/(b-y)$ diagram, their position agrees quite well with the 15 Myr isochrone, though their location is not exact. The 12 Myr isochrone only gives a poor fit for these stars, though again both isochrones fit the blue sequence well. We cannot place too much weight on the position of the red supergiants, because the reddening to the clus-

ter is very high, and the polynomial form used by Cardelli et al. (1989) introduces artificial bumpiness in the extinction curve (Maíz-Apellániz 2012).

In view of this, we take the cluster age to be $\tau = 14 \pm 2$ Myr, a range covering all isochrones that give a good fit to the dereddened M_V/c_0 plot. This age is almost identical to that found for the double cluster h and χ Per (Currie et al. 2010), as confirmed by the extremely similar distribution of spectral types at the top of the blue sequence. This age coincides with that found by Beauchamp et al. (1994), who used individual dereddening, but is younger than the values determined by both Joshi et al. (2008) and Subramanian et al. (2006).

3.3. Cluster mass

Our Strömgren photometry covers the whole range of B-type stars, in which we found 179 cluster members. Using the individual dereddened absolute magnitudes, M_V , we assigned a mass to each cluster member, by calibrating against the isochrone of Marigo et al. (2008). Of course, this procedure is only valid for stars without emission lines. Be stars cannot be individually dereddened and their apparent stellar parameters do not correspond to their actual mass (Fremat et al. 2005). They tend to be brighter than non-emission stars of the same spectral type by a factor that depends on rotational velocity and inclination angle (though they can be fainter when seen at high inclination; e.g., Townsend et al. 2004). Because the fraction of Be stars is very high in the cluster upper main-sequence, an accurate determination of the IMF is not possible, because the Be stars fall in bins with heavy weight.

We have tried to fit the IMF following the procedure of Maíz-Apellániz & Úbeda (2004), but our data cannot be adequately described by an exponential function. There are three reasons contributing to this. Firstly, our mass range is small and does not extend to sun-like stars. Second, differential reddening is very likely resulting in incompleteness for stars less massive than $\sim 5 M_\odot$. Third, there is a real excess of stars in the bins corresponding to ~ 8 to $10 M_\odot$. The same effect is clearly seen in the IMF determination of Beauchamp et al. (1994), which shows a lack of stars with masses around $5 M_\odot$ and an excess around $8 M_\odot$ (their Fig. 19). The lack of stars with intermediate mass is also visible in Fig. 16 of Joshi et al. (2008). This excess of stars around the turn-off might be caused by the large number of Be stars, because they would appear brighter (and hence more massive) than they really are because of two combined effects. On the one hand, fast rotation will make them slightly brighter than slower rotators of the same mass, as mentioned above. On the other hand, and perhaps more importantly, the dereddening procedure will overestimate their individual reddening, because the circumstellar excess would be taken for interstellar reddening. This over-correction of the interstellar reddening should result in brighter absolute magnitudes.

To correct for this possible effect, we repeated the IMF determination by assigning the average cluster reddening to the Be stars and then calculating M_V with the DM obtained from the isochrone fitting, but found no improvement to the fit. We then repeated the fit by adding 0.3 mag to their M_V to correct for the brightening caused by fast rotation. In all cases, we still found a lack of stars around $5 M_\odot$ and an excess of stars around $8 M_\odot$. Since our photometry does not extend to lower masses and we cannot fully exclude that this effect is real, we did not try to determine the slope of the IMF, and simply accepted the results from previous authors, who found that it approximates the

Salpeter value when the full range to solar-like stars is considered.

Our data, however, can be used to determine the total mass in B-type stars contained in the cluster (including Be stars), which is $M \approx 1\,200 \pm 100 M_{\odot}$, where the error bar reflects the uncertainty in assigning a mass to the Be stars. This value includes the B-type giants with an initial mass (M_{ini}) close to $\approx 14 M_{\odot}$ (but not the RSGs, which may have up to $M_{\text{ini}} \approx 14.5 M_{\odot}$) and the faintest objects in our sample with $\approx 3 M_{\odot}$. As mentioned, we are probably not complete for stars less massive than $5 M_{\odot}$. If we have $\approx 1\,000 M_{\odot}$ between 5 and $14 M_{\odot}$, where we are likely to be complete with 141 stars, a Miller & Scalo (1979) mass distribution implies $\sim 8\,000 M_{\odot}$ for the whole cluster. A Kroupa-type IMF implies a slightly higher mass. These are only rough estimates, but, together with the high number of B-type stars, they suggest that NGC 7419 is a moderately massive cluster with a total mass in the $5 - 10 \times 10^3 M_{\odot}$ range.

4. Discussion

We have presented for the first time Strömgren photometry and classification spectroscopy for B-type stars in NGC 7419. By using a large number of photometric standards in several young open clusters, we achieved a successful transformation to the standard system, even though the reddening to NGC 7419 is slightly higher than the reddening to any of our standard clusters. Since a correct transformation to the standard system requires the use of standard stars with similar intrinsic colours and similar reddenings to the target stars (Manfroid & Sterken 1987, Crawford 1994), there was an *a priori* risk of finding systematic effects in the transformed colours. Fortunately, the transformation was fully successful, as demonstrated by the excellent match between photometric and spectroscopic spectral types (see Sect. 3.2.2), showing that the standard clusters can be used to transform photometry of somewhat more reddened clusters.

Our distance estimate is higher than those of Joshi et al. (2008) and Subramanian et al. (2006). This is almost entirely due to the younger age estimated for the cluster, because the difference in the absolute magnitude of the turn-off at 14 Myr and 24 Myr is ≈ 0.5 mag (Marigo et al. 2008), resulting in a difference of ≈ 0.5 mag in DM . The observed spectral types fully support the younger age because no stars earlier than B2 should be observed at ages higher than 20 Myr.

The radial velocity of NGC 7419 corresponds to $v_{\text{LSR}} \approx -55 \text{ km s}^{-1}$ (Beauchamp et al. 1994). The dynamical distance for the cluster is thus ~ 4.5 kpc for the Galactic rotation curve of Reid et al. (2009), which agrees quite well with our distance determination. There are, however, very significant deviations from the Galactic rotation curve in this region (Reid et al. 2009). The open cluster NGC 7538 ($l = 111^{\circ}54$, $b = 0^{\circ}78$, $v_{\text{LSR}} = -57 \text{ km s}^{-1}$) has a parallax distance of 2.6 ± 0.2 kpc, but a kinematic distance of 4.6 kpc (Reid et al. 2009). To reduce the distance to NGC 7419 to a value similar to the parallax distance to NGC 7538, we would have to assume a very substantial departure from the standard reddening law, which does not seem to be borne out by either our photometry or that from Joshi et al. (2008).

Subramanian et al. (2006) assumed a standard reddening law with $R = 3.1$, while Joshi et al. (2008) calculated $R = 3.2 \pm 0.1$. The dereddening procedure of Crawford et al. (1970) implicitly assumes a reddening law similar to that in the solar neighbourhood. To confirm its validity, we plot the individual $E(b-y)$ values for all B-type stars never classified as Be stars against their

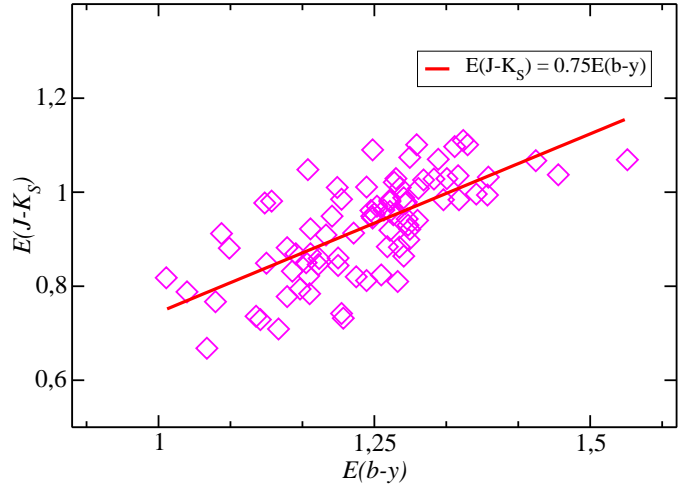


Fig. 11. $E(J - K_S)/E(b - y)$ diagram for normal B-type stars in the cluster. These points fit a straight line with a slope of 0.75.

$E(J - K_S)$ excesses in Fig. 11. The infrared excesses were calculated using their 2MASS photometry and the intrinsic colours for the photometric spectral type from Winkler (1997). Though the best-fit line, $E(J - K_S) = 0.75 \times E(b - y)$, is fully compatible within errors with a standard reddening law (for which values around 0.7 are expected for the slope of this relation), there is a large scatter around this line. Many stars have $E(J - K_S) \approx 0.1$ mag higher or lower than expected for their $E(b - y)$. This scatter is most likely dominated by photometric uncertainties, because the uncertainties in $E(J - K_S)$ is > 0.04 , even for the best 2MASS magnitudes.

4.1. Be stars

NGC 7419 presents the highest fraction of Be stars relative to the total number of B stars among all well-studied young open clusters in the Milky Way. The Be stars concentrate strongly above and around the main-sequence turn-off. Subramanian et al. (2006) suggested that most of the Be stars in the cluster were Herbig Be stars instead of classical Be stars. This seems very unlikely if we consider the following:

- Many Be stars present strong variability in their emission lines on time scales of years, including complete disappearance and reformation of the emission lines, a behaviour typical of classical Be stars and unreported in Herbig Be stars.
- The observed equivalent width of $H\alpha$ is $\gtrsim -50\text{\AA}$ in all our spectra or those in Malchenko & Tarasov (2011). These are values typical of early-type classical Be stars, while many Herbig Be stars present stronger emission.
- As discussed by Malchenko & Tarasov (2011), the Be stars in NGC 7419 present circumstellar excesses $E(J - K_S)$ in the range typical of classical Be stars in young open clusters. Most Herbig Be stars have much stronger excesses (Hillenbrand et al. 1992).
- The emission-line stars are very strongly concentrated towards the main-sequence turn-off, a characteristic typical of clusters containing classical Be stars (McSwain & Gies 2005). The distribution of Herbig Be stars, on the other hand, should follow the IMF, with the longer time-scale for disk dissipation favouring the detection of lower-mass systems. Moreover, a population of Herbig Be stars should be accompanied by the presence of lower mass pre-main sequence

stars, unless the IMF is utterly anomalous. Joshi et al. (2008) failed to detect any T Tauri star associated with the cluster.

In summary, we find no evidence for Herbig Be stars in the cluster and accordingly assume that all emission stars are classical Be stars.

4.2. Clusters with red supergiants

Clark et al. (2009b) carried out simulations of RSG populations by building synthetic clusters with masses of up to $4 \times 10^4 M_{\odot}$ by populating them according to a Kroupa (2001) IMF and evolving stars according to the solar metallicity evolutionary tracks of Meynet & Maeder (2000) with high initial rotation ($v_{\text{rot}} = 300 \text{ km s}^{-1}$). According to these simulations, a cluster with $3000 M_{\odot}$ is expected to have 1 ± 1 RSG at an age 12–15 Myr, while a $10000 M_{\odot}$ cluster is expected to have 2 ± 2 RSGs. The probability that a $5000 M_{\odot}$ cluster has zero RSGs at 14 Myr is $> 30\%$.

These numbers seem compatible with observations if one considers that even moderately massive clusters such as NGC 869 ($M_{\text{cl}} \approx 5000 M_{\odot}$ in the core; Currie et al. 2010) or NGC 663 do not contain any RSGs in their core regions, while NGC 884 (slightly less massive than NGC 869) contains one in the core region and four in the halo⁶. The five RSGs in NGC 7419, with a mass $\lesssim 10,000 M_{\odot}$, lie outside the $1\text{-}\sigma$ range derived from Monte-Carlo simulations, but well within the $2\text{-}\sigma$ range, even though no other cluster with a well-determined mass and a similar age contains more than two RSGs (Eggenberger et al. 2002).

We can thus assume that NGC 7419 represents the extreme tail of the statistical distribution. After all, the simulations use a particular set of evolutionary tracks with somewhat extreme conditions (a very high initial v_{rot}). However, the fact that it is also the Galactic cluster with the highest known fraction of Be stars in the upper main-sequence suggests the possibility of a physical reason for these phenomena.

The ratios of RSGs with respect to B-type stars and Be stars with respect to B stars seem to be correlated, and vary with metallicity (Meynet et al. 2007). The reasons for this correlation are unclear, because the ratio of RSGs to blue supergiants evolves with metallicity against theoretical expectations (Meynet et al. 2011). The metallicity of NGC 7419 is unlikely to be different from that of other clusters in its neighbourhood, though this should be checked with spectral modelling⁷. A high binary fraction may also have an impact on the number of RSGs, because stars in close binaries will undergo mass transfer during their evolution and never will grow to the size of a RSG.

Therefore we can propose a scenario where a cluster is formed with a low fraction of close binaries and thus angular momentum is not soaked up by binary motion, which results in very high initial v_{rot} for most stars. This scenario would explain the high fraction of Be stars and the high number of RSGs, because there would only be few binaries. However appealing such a scenario may be to explain the observed properties of NGC 7419, it cannot be taken as a rule for clusters with a high fraction of Be stars, as shown by the counterexample of NGC 663. This cluster, which has a total mass comparable to that of NGC 7419

⁶ Though the corresponding mass of the halo is difficult to evaluate. One could alternatively state that there are ten RSGs in the whole of the Perseus Double Cluster complex, which contains at least $20000 M_{\odot}$ (Currie et al. 2010).

⁷ Unfortunately, better (i.e., higher-resolution and higher-S/N) spectra than those displayed here are needed for this task.

(Pandey et al. 2005), also has a very high Be fraction around the main-sequence turn-off (Negueruela et al. 2005). Its nuclear region, on the other hand, does not contain any RSG, but five blue supergiants of spectral types B and early A. Again, we might be probing the tail of the statistical distribution, but it is quite striking to note that two well-studied⁸ clusters with similarly high fractions of Be stars present this widely different distribution of supergiants. In this sense, it is worthwhile noting that high rotational velocity can also be attained through mass transfer in a close binary (Marco et al. 2007, McSwain & Gies 2005), and so different physical mechanisms leading to the formation of Be stars may exist (see discussion in McSwain & Gies 2005 or Tarasov & Malchenko 2012).

It has also been claimed that the peculiarity of NGC 7419 is highly enhanced by the lack of any blue supergiant in the cluster, which makes its high number of RSGs still more unexpected (Beauchamp et al. 1994, Caron et al. 2003). The brightest blue star in the cluster, 103, was classified as B2.5 II-III by Caron et al. (2003), based on a far-red spectrum. Our spectral type, based on a classification spectrum, is quite similar, BC2 II, and places the object very close to the lower limit in luminosity for blue supergiants. A second object, 295, which had not been observed by previous authors because it is quite far away from the cluster core and very close to a much brighter foreground object, has a very similar spectrum, which we classify as BC2.5 Ib-II, though noting that the slightly different classifications may be due to the different resolutions used. In the dereddened CMD (Fig. 10), these two objects have an M_V slightly brighter than -5 mag, well above the cluster giants and ~ 2 mag brighter than the MS turn-off. Another member with as similar absolute magnitude is the blue straggler star 180, BN 0.5III. We can thus state that the lack of blue supergiants in NGC 7419 is partly a question of semantics, even though the ratio of RSGs to evolved blue stars is still extremely high when compared to other Galactic clusters (Eggenberger et al. 2002), confirming its uniqueness.

4.2.1. 2MASS diagram

The obscured clusters of red supergiants must be observed in the infrared, because heavy extinction renders them invisible at optical wavelengths. The line-of-sight to the clusters near the base of the Scutum arm is very complex, with many intervening populations that generate very heavy foreground contamination (Negueruela et al. 2012). The line-of-sight to NGC 7419 presents little contamination and the actual members can be selected from the Strömgren photometry. It is thus possible to create CMDs free from contamination to evaluate the effects of differential reddening and intrinsic dispersion.

Figure 12 displays the 2MASS $K_s/(J - K_s)$ diagram for stars selected as members of NGC 7419 from the analysis of the Strömgren photometry. The red supergiants are located on the upper right side of the diagram, clearly separated from the rest of the members that belong to the main sequence. The main sequence is very broad and dispersed, with $(J - K_s)$ ranging from ≈ 0.5 to 1.5 . This dispersion is, to a large degree, caused by a significant population of Be stars that present high $(J - K_s)$ excesses because of circumstellar disks. The excesses observed amongst the Be stars in NGC 7419 range from ~ 0 to ~ 0.5 , i.e., the same values as in field Be stars (Dougherty et al. 1994). However, the non-emission-line stars also present a very wide range of values.

⁸ NGC 7419 and NGC 663 are also sufficiently massive to be sure that the high fraction of Be stars is not due to small-number statistics. In both cases, we are considering > 150 B-type stars.

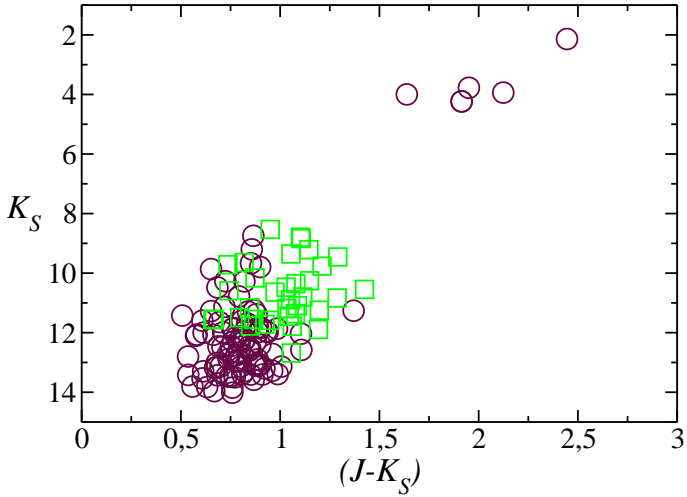


Fig. 12. K_S against $(J - K_S)$ for members of NGC 7419. Open squares represent Be stars in the cluster.

Figure 11 shows that the reddening follows a law close to the standard and thus the high dispersion must be caused by differential reddening, with $E(J - K_S)$ ranging from ~ 0.7 to ~ 1.1 .

The main sequence of NGC 7419 is difficult to trace in the $K_S/(J - K_S)$ diagram even though we removed all foreground contamination and the reddening to the cluster is only moderate. For the obscured clusters of red supergiants, the reddening is much higher, the foreground contamination is much heavier, and the longer distance results in smaller spatial extent and hence frequent blending at the spatial resolution of 2MASS. It is thus easy to understand why the main-sequence populations of these clusters have not been identified from 2MASS data.

4.2.2. Theoretical HR diagram for red supergiants

We can use the cluster parameters found in our analysis to evaluate the accuracy of cluster parameters derived exclusively from the RSG population, as has been done for several clusters (e.g., Davies 2007, Clark et al. 2009a, Negueruela et al. 2010). In Table 8, we present the 2MASS photometry for the five RSGs in NGC 7419. The errors in the determination of some magnitudes are high because of saturation problems, but we found no other broad-band near-infrared photometry for these stars in the literature. We derived the excesses in $(J - K_S)$ for each star taking the average intrinsic colours for each spectral type from González-Fernández & Negueruela (2012). Assuming standard reddening, $A_K = 0.67E(J - K_S)$, we calculated K_0 for each object. Then, we calculated M_K for each RSG, using the distance modulus for the cluster, $DM = 13.0$, determined in Section 3.2.1 from the analysis of Strömgren photometry. In obscured clusters, the distance is the most uncertain parameter, and must be estimated from the radial velocity (e.g., Davies 2007) or the run of extinction (e.g., Negueruela et al. 2011).

Finally, we used the following expressions, taken from Levesque et al. (2005), to calculate the intrinsic stellar parameters for the theoretical H-R diagram:

$$(J - K)_0 = 3.10 - 0.547(T_{\text{eff}}/1000 \text{ K}) \quad (4)$$

$$BC_K = 5.574 - 0.7589(T_{\text{eff}}/1000 \text{ K}) \quad (5)$$

$$(L/L_{\odot}) = 10^{-(M_{\text{bol}} - 4.74)/2.5} \quad (6)$$

The parameters determined are also listed in Table 8.

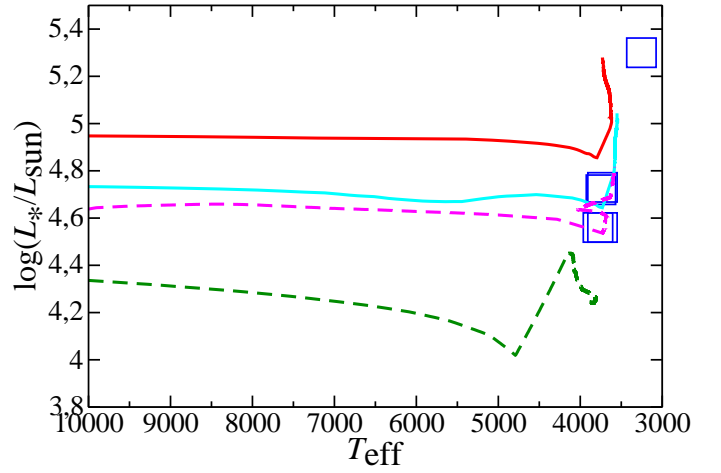


Fig. 13. HR diagram showing the locations of 5 RSGs in the cluster, with their positions derived from the spectral classification, assuming a distance to the cluster $d = 4.0$ kpc. We also plot isochrones from Meynet & Maeder (2000). The solid lines are the $\log t = 7.10$ (13 Myr; top, red), and $\log t = 7.20$ (16 Myr; bottom, blue) isochrones with high initial rotation. The dotted lines are the $\log t = 7.10$ (13 Myr; magenta), and $\log t = 7.20$ (16 Myr; green) isochrones without rotation. The size of the symbols represents the errors in $\log L_*$ that are due to observational uncertainties and calibration problems. The errors in T_{eff} , though difficult to quantify, should be smaller than the symbol size.

In Figure 13, we display the theoretical Hertzsprung-Russell (HR) diagram showing the positions of the five RSGs compared to different isochrones from Meynet & Maeder (2000). Their position appears to be consistent with the high rotation 16-Myr isochrone or the 13-Myr isochrone without rotation, but not with the 16-Myr isochrone without rotation. This is in excellent agreement with the 14-Myr age derived from the main-sequence turn-off, when we consider that a range of initial rotations is to be expected. In this theoretical HR diagram, the stars lie exactly at the expected positions for RSGs, confirming the idea that their somewhat awkward position in the $V/(b-y)$ diagram stems from the reddening procedure used for the isochrone⁹. The position of B950 lies beyond the end of the isochrone, at a much higher luminosity than that of the other four RSGs. This is not surprising given its exceptional nature (see next subsection), but we must also note that its 2MASS photometry is affected by very heavy saturation. In addition, this star presents strong mid-infrared excess (Fawley & Cohen 1974), and it is possible that its $E(J - K_S)$ excess is slightly overestimated, resulting in a too bright luminosity (L_*).

The excellent agreement of the theoretical isochrones with the positions of the RSGs provides further confirmation of the age determination. It also validates the use of similar diagrams to estimate the parameters of obscured clusters, for which the uncertainty in the distance clearly dominates all other sources of error.

4.3. MY Cep as a standard for late-M supergiants

Fawley & Cohen (1974) remarked on the peculiarity of B950 (IRC +60 375; generally known by its variable star designation,

⁹ The reddening procedure uses a Cardelli law, a polynomial approximation that introduces artificial bumpiness at high reddening (Maíz-Apellániz 2012).

Table 8. Photometric data for red supergiants in NGC 7419, from 2MASS.

Star	J	E_J	H	E_H	K_S	E_{K_S}	$E(J - K_S)$	M_K
B921=56	6.148	0.024	4.799	0.033	4.234	0.016	0.884	-9.358
B696=122	5.726	0.018	4.662	0.212	3.775	0.036	0.891	-9.822
B139	6.061	0.020	4.514	0.036	3.937	0.036	1.074	-9.783
B950	4.583	0.280	2.980	0.242	2.138	0.278	1.125	-11.616
B435	5.635	0.020	4.586	0.228	3.997	0.284	0.578	-9.390

MY Cep), because supergiants later than M4 were not known in open clusters (Abt 1963). Even such a luminous star as VY CMa, which is at or past the Hayashi limit (Wittkowski et al. 2012), has the spectral type M4–5 Ia⁺ (with some weak spectral variability). Confirmed supergiants with later spectral types are extremely rare (Wing 2009). VX Sgr shows pronounced variations in spectral type, from M4 Ia to ~M10 Ia. Solf (1978) remarked that its spectrum was similar to those of late-M giants, but showing stronger metallic lines, and suggested that this might be the defining characteristic of late-M supergiants. The spectrum of MY Cep seems to confirm this suggestion.

Another star with marked excursions in spectral type is S Per, a member of the Per OB1 association. This object spends most of its time as an M4 Ia supergiant, but it has been observed with spectral type as late as M8 (Wing 2009; and references therein). This object offers a good comparison to MY Cep, because the age of h & χ Per is believed to be very close to that of NGC 7419, and these two stars should have similar masses. MY Cep seems very unusual in that it permanently displays a late-M spectral type. Even though short excursions to other spectral types cannot be excluded, it seems to have varied by less than 0.5 spectral subtypes over the past ~ 60 years. The only known star displaying a similar behaviour is NML Cyg, which has been observed with a spectral type ~M6 Ia for the past ~ 50 years (Wing 2009). In view of this stability, NML Cyg and MY Cep could be taken as pseudo-standards for the classification of late-M supergiants, alleviating the lack of criteria discussed, among others, by Negueruela et al. (2012).

All late-M supergiants are surrounded by extended envelopes. VY CMa displays prominent ejecta that provides evidence for multiple and asymmetric mass loss events, and is surrounded by a dust envelope (Humphreys et al. 2007). An extended dust envelope has also been imaged around NML Cyg (Schuster et al. 2009). Maser mapping has allowed the detection of extended structures around S Per and VX Sgr and accurate distance determination for these sources via parallaxes (Asaki et al. 2010, Chen et al. 2007). Maser emission from MY Cep has also been detected. Several surveys have found SiO, OH, and water masers (Verheyen et al. 2012; and references therein), indicative of heavy mass loss and an extended envelope. Its spectral energy distribution in the mid-IR is very similar to that of S Per, though it suggests a smaller envelope (Fawley & Cohen 1974). According to the Padova evolutionary tracks (Marigo et al. 2008), MY Cep, which is close to the end of its life at 14 Myr, should have a mass ~14.5 M_{\odot} if it was born with a low rotational velocity.

5. Conclusions

By combining Strömgren photometry and classification spectra of its brightest stars, we have derived astrophysical parameters for the young open cluster NGC 7419. We obtained a distance of ~ 4 kpc, compatible with the kinematic distance implied from its radial velocity and the rotation curve of Reid et al. (2009), and

an age of 14 ± 2 Myr. The turn-off from the main sequence is found at spectral type B1, in excellent agreement with the age determination. The stellar population of NGC 7419 is similar to that of the double Perseus cluster, which has a similar age. We identified 179 B-type stars, covering the whole B1–B9 range, though differential reddening renders our sample incomplete for spectral types B6 and later.

We calibrated the mass of our stars from their absolute magnitudes by mapping them onto the corresponding isochrone. We found 141 stars between 5 and 14 M_{\odot} , implying a mass of ~ 1 000 M_{\odot} . Since previous authors have determined a mass distribution not far from Salpeter’s, this implies an initial mass approaching 5 000 M_{\odot} in stars more massive than the Sun. Extrapolation to lower masses results in a total initial mass close to 10 000 M_{\odot} , indicating that NGC 7419 is sufficiently massive to serve as a valid comparison for theoretical models and a template for the study of more obscured clusters.

We found a large population of Be stars, strongly concentrated around the main-sequence turn-off. Indeed, above the turn-off there are more Be stars than non-emission stars. The fraction of Be stars is $\approx 40\%$ above $V = 17$ (types B2 V and earlier) and very low for later types, confirming the trend seen in other clusters (McSwain & Gies 2005). Many of the Be stars in NGC 7419 have shown pronounced variability during the ~10 years of monitoring, with episodes of disk loss and reformation being reported here for the first time.

The 2MASS $K_S/(J - K_S)$ diagram for NGC 7419 shows no clearly defined sequence, even if only confirmed members are plotted. This is due to the combined effects of differential reddening, with $E(J - K_S)$ for non-emission B-type stars ranging from ≈ 0.7 to ≈ 1.1 mag, and the circumstellar excesses of Be stars, which may add up to ≈ 0.5 mag to $E(J - K_S)$. The reddening law is close to standard, and the dereddened 2MASS magnitudes of the M-type supergiants may be used to calculate their intrinsic parameters, which provide a very good fit to theoretical tracks, demonstrating the validity of this procedure to estimate the properties of obscured clusters.

The presence of five red supergiants in a cluster with $\lesssim 10\,000 M_{\odot}$ is only marginally consistent with population synthesis models (Clark et al. 2009b). When considered together with the very high fraction of Be stars and the very low ratio of evolved blue stars to RSGs, it strongly hints at the presence of some physical mechanism, perhaps related to high initial rotational velocities, as the source of these effects. Finally, MY Cep has the latest spectral type of all known cluster RSGs, at M7.5 I, and presents clear evidence for heavy mass loss. Unlike other extreme RSGs, it does not seem to have undergone any substantial spectral variability over the past 60 years, which makes it an important pseudo-standard to classify very late RSGs.

Acknowledgements. We thank the referee, Radostin Kurtev, for his helpful comments.

This research is partially supported by the Spanish Ministerio de Ciencia e Innovación (MICINN) under grants AYA2010-21697-C05-05 and CSD2006-70, and by the Generalitat Valenciana (ACOMP/2012/134).

The WHT is operated on the island of La Palma by the Isaac Newton Group in the Spanish Observatorio del Roque de Los Muchachos of the Instituto de Astrofísica de Canarias. Partly based on observations made with the Nordic Optical Telescope, operated on the island of La Palma jointly by Denmark, Finland, Iceland, Norway, and Sweden, in the Spanish Observatorio del Roque de los Muchachos of the Instituto de Astrofísica de Canarias. Some of the data have been taken using ALFOSC, which is owned by the Instituto de Astrofísica de Andalucía (IAA) and operated at the Nordic Optical Telescope under agreement between IAA and the NBIFAFG of the Astronomical Observatory of Copenhagen. Based in part on observations made at Observatoire de Haute Provence (CNRS), France.

This research has made use of the Simbad database, operated at CDS, Strasbourg (France) and of the WEBDA database, operated at the Institute for Astronomy of the University of Vienna. This publication makes use of data products from the Two Micron All Sky Survey, which is a joint project of the University of Massachusetts and the Infrared Processing and Analysis Center/California Institute of Technology, funded by the National Aeronautics and Space Administration and the National Science Foundation.

References

- Abt, H.A. 1963, *ApJS*, 8, 99
 Abt, H.A., & Levato, H. 1997, *PASP*, 89, 648A
 Asaki, Y., Deguchi, S., Imai, H., et al. 2010, *ApJ*, 721, 267
 Beauchamp, A., Moffat, A.F.J., & Drissen, L. 1994, *ApJS*, 93, 187
 Blanco, V., Nassau, J.J., Stock, J., & Wehlau, W. 1955, *ApJ*, 121, 63
 Canterna, R., Perry, C. L., & Crawford, D. L. 1979, *PASP*, 91, 263
 Cardelli, J.A., Clayton, G.C., & Mathis, J.S. 1989, *ApJ*, 345, 245
 Caron, G., Moffat, A.F.J., St-Louis, N., et al. 2003, *AJ*, 126, 1415
 Chen, X., Shen, Z.-Q., & Xu, Y. 2007, *ChJAA*, 7, 531
 Clark, J.S., Negueruela, I., Davies, B., et al. 2009a, *A&A*, 498, 109
 Clark, J.S., Davies, B., Najarro, F., et al. 2009b, *A&A*, 498, 109
 Crawford, D.L., & Mander, J. 1966, *AJ*, 71, 114
 Crawford, D.L., & Barnes, J.V. 1970, *AJ*, 75, 978
 Crawford, D.L., Glaspey, J. W., & Perry, C.L. 1970, *AJ*, 75, 822
 Crawford, D.L., Barnes, J.V., & Hill, G. 1977, *AJ*, 82, 606
 Crawford, D.L. 1978, *AJ*, 83, 48
 Crawford, D.L. 1994, *PASP*, 106, 397
 Currie, T., Hernandez, J., Irwin, J., et al. 2010, *ApJS*, 186, 191
 Davies, B., Figer, D.F., Kudritzki, R.P., et al. 2007, *ApJ*, 671, 781
 Delgado, A.J., & Alfaro, E.J. 1989, *A&A*, 219, 121
 Draper, P.W., Taylor, M., & Allan, A. 2000, *Starlink User Note 139.12*, R.A.L.
 Dougherty, S.M., Waters, L.B.F.M., Burki, G., et al. 1994, *A&A*, 290, 609
 Eggenberger, P., Meynet, G., & Maeder, A. 2002, *A&A*, 386, 576
 Fawley, W.M., & Cohen, M. 1974, *ApJ*, 193, 367
 Figer, D.F., MacKenty, J.W., Robberto, M., et al. 2006, *ApJ*, 643, 1166
 Frémat, Y., Zorec, J., Hubert, A.M., & Floquet, M. 2005, *A&A*, 440, 305
 Girardi, L., Delcanton, J., Williams, B., et al. 2008, *PASP*, 120, 583
 González-Fernández, C., & Negueruela, I. 2012, *A&A*, 539, 100
 Hillenbrand, L.A., Strom, S.E., Vrba, F.J., & Keene, J. 1992, *ApJ*, 397, 613
 Hoag, A.A., & Applequist, L. 1965, *ApJS*, 12, 215
 Howarth, I., Murray, J., Mills, D., & Berry, D.S. 1998, *Starlink User Note 50.21*, R.A.L.
 Huang, W., & Gies, D.R. 2006, *ApJ* 648, 580
 Humphreys, R.M., Helton, L.A., & Jones, T.J. 2007, *AJ*, 133, 2716
 Johnson, H.L., & Morgan, W.W. 1955, *ApJ*, 122, 429
 Joshi, H., Kumar, B., Singh, K.P., et al. 2008, *MNRAS*, 391, 1279
 Keenan, P.C. & Hynek, J.A. 1945, *ApJ*, 101, 265
 Kroupa, P. 1998, *ASPC*, 134, 483
 Kroupa, P. 2001, *MNRAS*, 322, 231
 Levesque, E.M., Massey, P., Olsen, K.A.G., et al. 2005, *ApJ*, 628, 973
 McSwain, M.V., & Gies, D.R. 2005, *ApJS*, 161, 118
 Maíz Apellániz, J., & Úbeda, L. 2005, *ApJ*, 629, 873
 Maíz-Apellániz, J. 2012, [arXiv:1209.2560](https://arxiv.org/abs/1209.2560)
 Maeder, A. 1990 *A&AS*, 84, 139
 Malchenko, S.L., & Tarasov, A.E. 2011, *Astrophysics*, 54, No. 1, 63.
 Meynet, G., & Maeder, A. 2000, *A&A*, 361, 101
 Manfroid, J., & Sterken, C. 1987, *A&A*, 71, 539
 Manfroid, J. 1993, *A&A*, 271, 714
 Marco, A., & Bernabeu, G. 2001, *A&A*, 372, 477
 Marco, A., Negueruela, I., & Motch, C. 2007, in *Active OB-Stars: Laboratories for Stellar and Circumstellar Physics*, ASP Conference Series, Vol. 361, Proceedings of the conference held 29 August - 2 September, 2005 at Hokkaido University, Sapporo, Japan. Edited by S. Stefl, S. P. Owocki, and A. T. Okazaki. San Francisco: Astronomical Society of the Pacific, 2007, p.388
 Marigo, P., Girardi, L., Bressan, A., et al. 2008, *A&A*, 482, 883
 Mermilliod, J.C., Mayor, M., & Udry, S. 2008, *A&A*, 485, 303
 Meynet, G., & Maeder, A. 2000, *A&A*, 361, 101
 Meynet, G., Eggenberger, P., & Maeder, A. 2007, in *Stellar Populations as Building Blocks of Galaxies*. Proceedings of IAU Symposium 241. Edited by A. Vazdekis and R.F. Peletier. Cambridge: Cambridge University Press, 2007, pp.13-22
 Meynet, G., Georgy, C., Hirschi, R., et al. 2011, *BSRSL*, 80, 266
 Miller, G.E., & Scalo, J.M. 1979, *ApJS*, 41, 513
 Morgan, W.W., & Harris, D.L. 1956, *Vistas Astron.*, 2, 1124
 Negueruela, I., Motch, C., & Herant, O., & Marco, A. 2005, *Be Newsletter*, 37, 22
 Negueruela, I., González-Fernández, C., Marco, A., et al. 2010, *A&A*, 513, A74
 Negueruela, I., González-Fernández, C., Marco, A., & Clark, J.S. 2011, *A&A*, 528, A59
 Negueruela, I., Marco, A., González-Fernández, C., et al. 2012, *A&A*, 547, 15
 O'Donnell, J.E. 1994, *ApJ*, 422, 158
 Pandey, A.K., Upadhyay, K., Ogura, K., et al. 2005, *MNRAS*, 358, 1290
 Perry, C.L., Lee, P.D., & Barnes, J.V. 1978, *PASP*, 90, 73
 Perry, C.L., Olsen, E.H., & Crawford, D.L. 1987, *PASP*, 99, 1184
 Pigulski, A., & Kopacki, G. 2000, *A&AS*, 146, 465
 Porter, J.M., & Rivinius, T. 2003, *PASP*, 115, 1153
 Reid, M.J., Menten, K.M., Zheng, X.W., et al. 2009, *ApJ*, 700, 137
 Saesen, S., Carrier, F., Pigulski, A., et al. 2010a, *A&A*, 515A, 16S
 Saesen, S., Pigulski, A., Carrier, F., et al. 2010b, *Astron. Nachr.*, 331, 1080S
 Shortridge, K., Meyerdicks, H., Currie, M., et al. 1997, *Starlink User Note 86.15*, R.A.L.
 Schild, R.E. 1965, *ApJ*, 142, 979
 Schuster, M.T., Marengo, M., Hora, J.L., et al. 2009, *ApJ*, 669, 1423
 Skrutskie, M.F., Cutri, R.M., & Stiening, R. 2006, *AJ*, 131, 1163
 Slesnick C.L., Hillenbrand L.A., & Massey P. 2002, *ApJ*, 576, 880
 Slettebak, A. 1968, *ApJ*, 154, 933
 Solf, A.J. 1978, *A&AS*, 34, 409
 Stetson, P.B. 1987, *PASP*, 99, 191
 Subramanian, A., Mathew, B., Bhatt, B.C., & Ramya, S. 2006, *MNRAS*, 370, 743
 Tarasov, A.E., & Malchenko, S.L. 2012, *Astronomy Letters*, 38, No.7, 428
 Townsend, R.H.D., Owocki, S.P., & Howarth, I.D. 2004, *MNRAS*, 350, 189
 Turner, D., Moffat, A.F.J., Lamontagne, R., et al. 1983, *AJ*, 88, 1199
 Verheyen, L., Messineo, M., & Menten, K.M. 2012, *A&A*, 541, A36
 Walborn, N.R., & Fitzpatrick, E.L. 1990, *PASP*, 102, 379
 Wing, R.F. 2009, in *The Biggest, Baddest, Coolest Stars*, ed. D.G. Luttermoser, B.J. Smith, & R.E. Stencel. ASP Conf. Ser. 412, 113
 Winkler, H. 1997, *MNRAS*, 287, 481
 Wittkowski, M., Hauschildt, P.H., Arroyo-Torres, B., & Marcaide, J.M. 2012, *A&A*, 540, L12

Table 3. Photometry and coordinates for stars in the field of NGC 7419.

Name	Name(WEBDA)	α (J2000)	δ (J2000)	V	σ_V	$(b - y)$	$\sigma_{(b-y)}$	c_1	σ_{c_1}	N
2	456	22 54 38.42	+60 45 33.80	18.140	0.038	1.089	0.049	0.994	0.088	1
4	1595	22 54 10.55	+60 45 37.20	17.515	0.037	1.099	0.048	0.382	0.075	1
5	1593	22 54 04.67	+60 45 40.31	17.406	0.037	1.167	0.048	0.537	0.076	1
6	1594	22 54 22.27	+60 45 40.70	16.209	0.007	1.221	0.004	0.307	0.097	4
8	1592	22 54 04.19	+60 45 43.00	16.103	0.016	0.672	0.019	0.224	0.056	4
9	390	22 54 31.55	+60 45 44.70	18.187	0.037	1.229	0.048	0.853	0.084	1

Table 4. 2MASS photometry for member stars of NGC 7419.

Name	J	σ_J	H	σ_H	K_S	σ_{K_S}
B-type stars						
2	14.318	0.030	13.757	0.035	13.407	0.038
4	13.743	0.028	13.214	0.031	12.964	0.033
5	12.851	0.036	12.250	0.039	11.867	0.035
6	12.113	0.021	11.529	0.022	11.244	0.020
9	14.003	0.031	13.380	0.031	13.119	0.034
Supergiants						
56	6.148	0.024	4.799	0.033	4.234	0.016
122	5.726	0.018	4.662	0.212	3.775	0.036
B139	6.061	0.020	4.514	0.036	3.937	0.036
B435	5.635	0.020	4.586	0.228	3.997	0.284
B397	4.583	0.280	2.980	0.242	2.138	0.278
Be type stars						
18	11.503	0.021	10.887	0.020	10.473	0.019
30	13.086	0.023	12.373	0.020	11.893	0.020
34	12.642	0.020	12.052	0.022	11.719	0.019
44	10.454	0.020	9.958	0.020	9.717	0.019
47	12.442	0.019	11.747	0.022	11.245	0.020

Table 7. Photometry for membership of NGC 7419.

Name	$E(b - y)$	M_V	Spectral Type(photometric)
2	1.131	0.278	(B8–B9) V
4	1.201	–0.648	B1.5 V
5	1.255	–0.990	(B2.5–B3) V
6	1.334	–2.526	B1 V
9	1.287	–0.349	(B7–B8) V